

First Principles Model of Electric Cable Braid Penetration with Dielectrics

Salvatore Campione*, Larry K. Warne, William L. Langston, and Lorena I. Basilio

Abstract—In this paper, we report the formulation to account for dielectrics in a first principles multipole-based cable braid electromagnetic penetration model. To validate our first principles model, we consider a one-dimensional array of wires, which can be modeled analytically with a multipole-conformal mapping expansion for the wire charges; however, the first principles model can be readily applied to realistic cable geometries. We compare the elastance (i.e., the inverse of the capacitance) results from the first principles cable braid electromagnetic penetration model to those obtained using the analytical model. The results are found in good agreement up to a radius to half spacing ratio of 0.5–0.6, depending on the permittivity of the dielectric used, within the characteristics of many commercial cables. We observe that for typical relative permittivities encountered in braided cables, the transfer elastance values are essentially the same as those of free space; the self-elastance values are also approximated by the free space solution as long as the dielectric discontinuity is taken into account for the planar mode.

1. INTRODUCTION

Understanding electromagnetic pathways into critical components is essential in determining potential damage or upset due to electromagnetic coupling. One important pathway into components is electromagnetic penetration through braided shields used in cables. Braided cables are generally modeled via transfer parameters (impedance Z_T and admittance Y_T , which model the shield properties related to the braid weave characteristics and material) and self-parameters (impedance Z_c and admittance Y_c , which are formed by the inner conductor and the shield) [1–8], which are then used in a transmission line formalism [9].

Recently, a first principles multipole-based cable braid electromagnetic penetration model has been proposed in [5, 6, 10] to compute the transfer and self-parameters of a shielded cable; the electric penetration case without dielectrics was recently compared to an analytical solution in [11]. The first principles model delivers results that are dependent on the actual geometry of the cable in question enabling one to also account for non-standard braid weave patterns or non-ideal geometric variations. In this paper, we limit our analysis to the case of electric penetration in the presence of dielectrics (not considered in [11]), and in particular to the determination of the internal and external potentials ϕ_c and ϕ_b (more details are given in later sections) that will be used to determine the transfer capacitance C_T and the self-capacitance C_1 . Generally, C_T is computed via the complete semi-empirical model assembled by Kley [12] based on canonical models augmented by measurements of typical commercial cables. For model verification, we will use our first principles model on a canonical structure, namely a one-dimensional array of wires, which can be modeled analytically through a multipole-conformal mapping expansion for the wire charges. However, the first principles model can be readily applied to realistic cable geometries, as we did for example in [11].

Received 30 October 2017, Accepted 14 February 2018, Scheduled 25 February 2018

* Corresponding author: Salvatore Campione (sncampi@sandia.gov).

The authors are with the Electromagnetic Theory Department, Sandia National Laboratories, Albuquerque, NM 87185, USA.

2. IMAGE METHOD TO ACCOUNT FOR EFFECTS OF DIELECTRICS IN THE FIRST PRINCIPLES METHOD

Consider the electric problem when dielectric materials are present. With the approximate local planar model (where the cylindrical geometry is approximated by a local plane geometry) we take two dielectric half spaces with permittivities ε_1 and ε_2 about the braid as shown in Fig. 1, with the dielectric interfaces being at $y = h_1$ and $y = -h_2$. Note that the wires have radius a and period $2w$, and are located in a material with permittivity ε_0 . Moreover, the ε_1 dielectric represents the inner region of the cable, whereas the ε_2 dielectric represents the outer jacket.

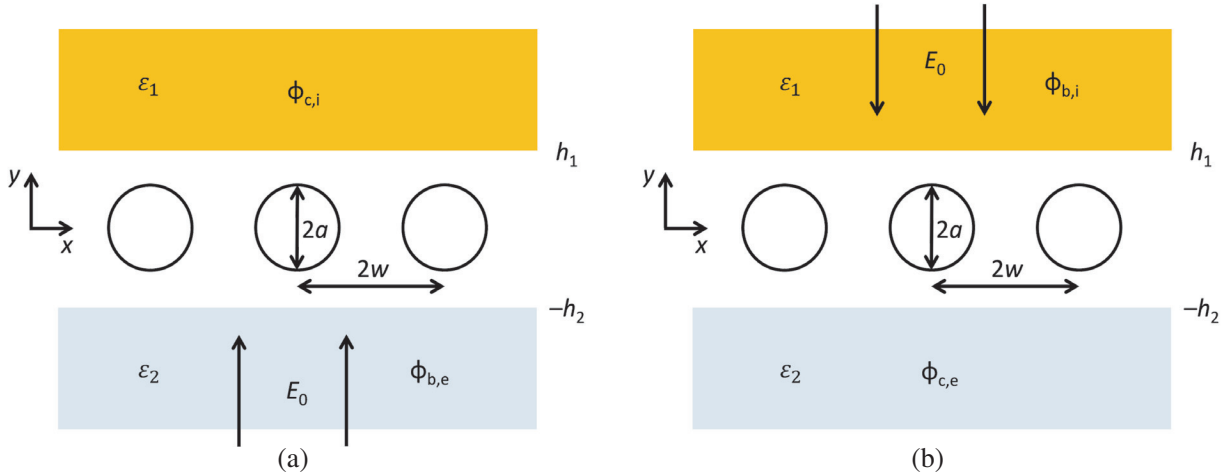


Figure 1. Dielectric materials surround the planar braid layer: (a) excitation from below and (b) excitation from above. $\phi_{c,i}$ and $\phi_{c,e}$ represent the internal and external potentials in the shadow side of the structure, respectively. $\phi_{b,i}$ and $\phi_{b,e}$ represent the internal and external potentials in the illuminated side of the structure, respectively.

We first decompose the total field into a uniform electric displacement $D = \varepsilon E$ in the y direction in addition to a field generated by the multipolar charges. Because we are representing the braid wires by line multipole moment segments [5, 6, 10, 11], these charge multipoles can be imaged in the dielectric interfaces to represent the potential in the various regions. In other words, the potential computed in [11] will be scaled according to what is described next.

Let us consider a charge q in the center region at $y = 0$, and the dielectric interfaces are at $y = h_1$ and $y = -h_2$ with respect to the charge position as depicted in Fig. 2.

When driven from below, $D_0 = \varepsilon_2 E_0$ and the incident uniform field potential can be written as

$$\phi_{inc} = \begin{cases} -yE_a & -h_2 \leq y \leq h_1 \\ -(y - h_1)E_a \frac{\varepsilon_0}{\varepsilon_1} - h_1E_a & y \geq h_1 \\ -(y + h_2)E_a \frac{\varepsilon_0}{\varepsilon_2} + h_2E_a & y \leq -h_2 \end{cases} \quad (1)$$

with $\varepsilon_0 E_a = \frac{\varepsilon_1 D_0}{\varepsilon_1 + \varepsilon_2}$ (see Appendix A for its derivation and a discussion of the solution of the problem given as the superposition of two problems). When driven from above, $D_0 = \varepsilon_1 E_0$ and the incident uniform field potential can be written as

$$\phi_{inc} = \begin{cases} yE_a & -h_2 \leq y \leq h_1 \\ (y - h_1)E_a \frac{\varepsilon_0}{\varepsilon_1} + h_1E_a & y \geq h_1 \\ (y + h_2)E_a \frac{\varepsilon_0}{\varepsilon_2} - h_2E_a & y \leq -h_2 \end{cases} \quad (2)$$

with $\varepsilon_0 E_a = \frac{\varepsilon_2 D_0}{\varepsilon_1 + \varepsilon_2}$ (derived similarly to what is shown in Appendix A).

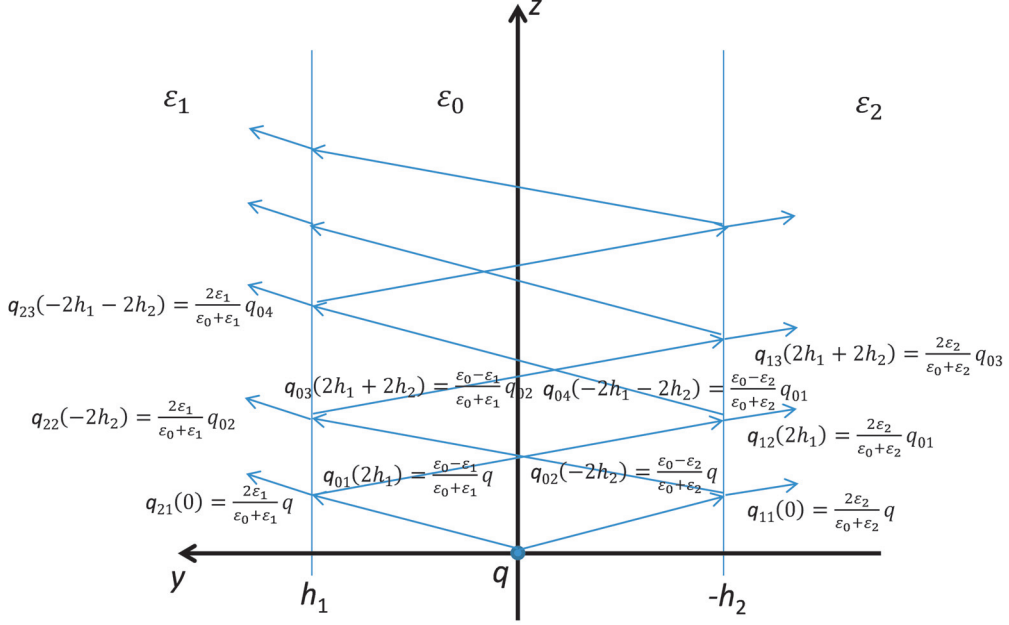


Figure 2. Schematic illustration of the image method to account for the image charges.

Following the procedure described in [13–15], the potential in the central region containing the wires with permittivity ϵ_0 can be computed as a summation of the direct contribution from the charge, plus the multiple reflections from the two dielectric boundaries at h_1 (terms q_{01} , q_{03} , etc. indicated in Fig. 2) and $-h_2$ (terms q_{02} , q_{04} , etc. indicated in Fig. 2). In other words, the potential in the central region is given by

$$\begin{aligned}
 \frac{4\pi\epsilon_0}{q}\phi = & \frac{1}{\sqrt{x^2 + y^2 + z^2}} + \frac{\epsilon_0 - \epsilon_1}{\epsilon_0 + \epsilon_1} \frac{1}{\sqrt{x^2 + (y - 2h_1)^2 + z^2}} + \frac{\epsilon_0 - \epsilon_2}{\epsilon_0 + \epsilon_2} \frac{1}{\sqrt{x^2 + (y + 2h_2)^2 + z^2}} \\
 & + \frac{\epsilon_0 - \epsilon_1}{\epsilon_0 + \epsilon_1} \frac{\epsilon_0 - \epsilon_2}{\epsilon_0 + \epsilon_2} \frac{1}{\sqrt{x^2 + (y + 2h_1 + 2h_2)^2 + z^2}} + \frac{\epsilon_0 - \epsilon_2}{\epsilon_0 + \epsilon_2} \frac{\epsilon_0 - \epsilon_1}{\epsilon_0 + \epsilon_1} \frac{1}{\sqrt{x^2 + (y - 2h_1 - 2h_2)^2 + z^2}} \\
 & + \left(\frac{\epsilon_0 - \epsilon_1}{\epsilon_0 + \epsilon_1}\right)^2 \frac{\epsilon_0 - \epsilon_2}{\epsilon_0 + \epsilon_2} \frac{1}{\sqrt{x^2 + (y - 4h_1 - 2h_2)^2 + z^2}} \\
 & + \left(\frac{\epsilon_0 - \epsilon_2}{\epsilon_0 + \epsilon_2}\right)^2 \frac{\epsilon_0 - \epsilon_1}{\epsilon_0 + \epsilon_1} \frac{1}{\sqrt{x^2 + (y + 2h_1 + 4h_2)^2 + z^2}} \\
 & + \left(\frac{\epsilon_0 - \epsilon_1}{\epsilon_0 + \epsilon_1}\right)^2 \left(\frac{\epsilon_0 - \epsilon_2}{\epsilon_0 + \epsilon_2}\right)^2 \frac{1}{\sqrt{x^2 + (y + 4h_1 + 4h_2)^2 + z^2}} \\
 & + \left(\frac{\epsilon_0 - \epsilon_2}{\epsilon_0 + \epsilon_2}\right)^2 \left(\frac{\epsilon_0 - \epsilon_1}{\epsilon_0 + \epsilon_1}\right)^2 \frac{1}{\sqrt{x^2 + (y - 4h_1 - 4h_2)^2 + z^2}} \\
 & + \left(\frac{\epsilon_0 - \epsilon_1}{\epsilon_0 + \epsilon_1}\right)^3 \left(\frac{\epsilon_0 - \epsilon_2}{\epsilon_0 + \epsilon_2}\right)^2 \frac{1}{\sqrt{x^2 + (y - 6h_1 - 4h_2)^2 + z^2}} \\
 & + \left(\frac{\epsilon_0 - \epsilon_2}{\epsilon_0 + \epsilon_2}\right)^3 \left(\frac{\epsilon_0 - \epsilon_1}{\epsilon_0 + \epsilon_1}\right)^2 \frac{1}{\sqrt{x^2 + (y + 4h_1 + 6h_2)^2 + z^2}} + \dots
 \end{aligned} \tag{3}$$

Note if there is no outer dielectric jacket material, $\varepsilon_2 = \varepsilon_0$, we end up with only two terms (the source and one image in ε_1).

In a similar way to Eq. (3), taking into account the multiple reflections in Fig. 2 (terms q_{21} , q_{22} , q_{23} , etc.), the potential in the region with permittivity ε_1 is given by

$$\begin{aligned} \frac{4\pi\varepsilon_1}{q}\phi = & \frac{2\varepsilon_1}{\varepsilon_0 + \varepsilon_1} \frac{1}{\sqrt{x^2 + y^2 + z^2}} + \frac{2\varepsilon_1}{\varepsilon_0 + \varepsilon_1} \frac{\varepsilon_0 - \varepsilon_1}{\varepsilon_0 + \varepsilon_1} \frac{\varepsilon_0 - \varepsilon_2}{\varepsilon_0 + \varepsilon_2} \frac{1}{\sqrt{x^2 + (y + 2h_1 + 2h_2)^2 + z^2}} \\ & + \frac{2\varepsilon_1}{\varepsilon_0 + \varepsilon_1} \left(\frac{\varepsilon_0 - \varepsilon_1}{\varepsilon_0 + \varepsilon_1} \right)^2 \left(\frac{\varepsilon_0 - \varepsilon_2}{\varepsilon_0 + \varepsilon_2} \right)^2 \frac{1}{\sqrt{x^2 + (y + 4h_1 + 4h_2)^2 + z^2}} \\ & + \frac{2\varepsilon_1}{\varepsilon_0 + \varepsilon_1} \left(\frac{\varepsilon_0 - \varepsilon_1}{\varepsilon_0 + \varepsilon_1} \right)^3 \left(\frac{\varepsilon_0 - \varepsilon_2}{\varepsilon_0 + \varepsilon_2} \right)^3 \frac{1}{\sqrt{x^2 + (y + 6h_1 + 6h_2)^2 + z^2}} + \dots \\ & + \frac{2\varepsilon_1}{\varepsilon_0 + \varepsilon_1} \frac{\varepsilon_0 - \varepsilon_2}{\varepsilon_0 + \varepsilon_2} \frac{1}{\sqrt{x^2 + (y + 2h_2)^2 + z^2}} \\ & + \frac{2\varepsilon_1}{\varepsilon_0 + \varepsilon_1} \left(\frac{\varepsilon_0 - \varepsilon_2}{\varepsilon_0 + \varepsilon_2} \right)^2 \frac{\varepsilon_0 - \varepsilon_1}{\varepsilon_0 + \varepsilon_1} \frac{1}{\sqrt{x^2 + (y + 2h_1 + 4h_2)^2 + z^2}} \\ & + \frac{2\varepsilon_1}{\varepsilon_0 + \varepsilon_1} \left(\frac{\varepsilon_0 - \varepsilon_2}{\varepsilon_0 + \varepsilon_2} \right)^3 \left(\frac{\varepsilon_0 - \varepsilon_1}{\varepsilon_0 + \varepsilon_1} \right)^2 \frac{1}{\sqrt{x^2 + (y + 4h_1 + 6h_2)^2 + z^2}} \\ & + \frac{2\varepsilon_1}{\varepsilon_0 + \varepsilon_1} \left(\frac{\varepsilon_0 - \varepsilon_2}{\varepsilon_0 + \varepsilon_2} \right)^4 \left(\frac{\varepsilon_0 - \varepsilon_1}{\varepsilon_0 + \varepsilon_1} \right)^3 \frac{1}{\sqrt{x^2 + (y + 6h_1 + 8h_2)^2 + z^2}} + \dots \end{aligned} \quad (4)$$

and the potential in the region with permittivity ε_2 (terms q_{11} , q_{12} , q_{13} , etc. indicated in Fig. 2) is given by

$$\begin{aligned} \frac{4\pi\varepsilon_2}{q}\phi = & \frac{2\varepsilon_2}{\varepsilon_0 + \varepsilon_2} \frac{1}{\sqrt{x^2 + y^2 + z^2}} + \frac{2\varepsilon_2}{\varepsilon_0 + \varepsilon_2} \frac{\varepsilon_0 - \varepsilon_2}{\varepsilon_0 + \varepsilon_2} \frac{\varepsilon_0 - \varepsilon_1}{\varepsilon_0 + \varepsilon_1} \frac{1}{\sqrt{x^2 + (y - 2h_1 - 2h_2)^2 + z^2}} \\ & + \frac{2\varepsilon_2}{\varepsilon_0 + \varepsilon_2} \left(\frac{\varepsilon_0 - \varepsilon_2}{\varepsilon_0 + \varepsilon_2} \right)^2 \left(\frac{\varepsilon_0 - \varepsilon_1}{\varepsilon_0 + \varepsilon_1} \right)^2 \frac{1}{\sqrt{x^2 + (y - 4h_1 - 4h_2)^2 + z^2}} \\ & + \frac{2\varepsilon_2}{\varepsilon_0 + \varepsilon_2} \left(\frac{\varepsilon_0 - \varepsilon_2}{\varepsilon_0 + \varepsilon_2} \right)^3 \left(\frac{\varepsilon_0 - \varepsilon_1}{\varepsilon_0 + \varepsilon_1} \right)^3 \frac{1}{\sqrt{x^2 + (y - 6h_1 - 6h_2)^2 + z^2}} + \dots \\ & + \frac{2\varepsilon_2}{\varepsilon_0 + \varepsilon_2} \frac{\varepsilon_0 - \varepsilon_1}{\varepsilon_0 + \varepsilon_1} \frac{1}{\sqrt{x^2 + (y - 2h_1)^2 + z^2}} \\ & + \frac{2\varepsilon_2}{\varepsilon_0 + \varepsilon_2} \left(\frac{\varepsilon_0 - \varepsilon_1}{\varepsilon_0 + \varepsilon_1} \right)^2 \frac{\varepsilon_0 - \varepsilon_2}{\varepsilon_0 + \varepsilon_2} \frac{1}{\sqrt{x^2 + (y - 4h_1 - 2h_2)^2 + z^2}} \\ & + \frac{2\varepsilon_2}{\varepsilon_0 + \varepsilon_2} \left(\frac{\varepsilon_0 - \varepsilon_1}{\varepsilon_0 + \varepsilon_1} \right)^3 \left(\frac{\varepsilon_0 - \varepsilon_2}{\varepsilon_0 + \varepsilon_2} \right)^2 \frac{1}{\sqrt{x^2 + (y - 6h_1 - 4h_2)^2 + z^2}} \\ & + \frac{2\varepsilon_2}{\varepsilon_0 + \varepsilon_2} \left(\frac{\varepsilon_0 - \varepsilon_1}{\varepsilon_0 + \varepsilon_1} \right)^4 \left(\frac{\varepsilon_0 - \varepsilon_2}{\varepsilon_0 + \varepsilon_2} \right)^3 \frac{1}{\sqrt{x^2 + (y - 8h_1 - 6h_2)^2 + z^2}} + \dots \end{aligned} \quad (5)$$

Note that the multipolar coefficients of dipole and octupole in the reflection terms (i.e., with a term $\frac{\varepsilon_0 - \varepsilon_1}{\varepsilon_0 + \varepsilon_1}$ or $\frac{\varepsilon_0 - \varepsilon_2}{\varepsilon_0 + \varepsilon_2}$) will be further multiplied by -1 to guarantee continuity of both potential and normal

displacement at the two dielectric interfaces; note that in terms with even numbers of such coefficients, generated by multiple reflections, these negative signs will cancel.

When illuminating from below, for the shadow side of the structure, we evaluate a total potential far from the braid to find $\phi \rightarrow \phi_{c,i}$. For the illuminated side of the structure, we evaluate the potential far from the braid to find $\phi \rightarrow \phi_{inc} + \phi_{b,e}$. Normalizing by the drive $E_0 = D_0/\varepsilon_0$, we find the desired internal $\phi_{c,i}/E_0$ and external $\phi_{b,e}/E_0$. When illuminating from above, for the shadow side of the structure, we evaluate a total potential far from the braid to find $\phi \rightarrow \phi_{c,e}$. For the illuminated side of the structure, we evaluate the potential far from the braid to find $\phi \rightarrow \phi_{inc} + \phi_{b,i}$. Normalizing by the drive $E_0 = D_0/\varepsilon_0$, we find the desired external $\phi_{c,e}/E_0$ and internal $\phi_{b,i}/E_0$.

3. ANALYTIC TEST CASE: ONE-DIMENSIONAL ARRAY OF WIRES ON TOP OF A DIELECTRIC HALF SPACE

The problem of field leakage through an array of cylinders is the basic canonical periodic shield [16], for which simple analytical solutions are available when the cylinder radius is small compared with the spacing [3, 17, 18]; an accurate bipolar solution approximation to the elastance (which holds for all ratios of radius to spacing) was recently reported in [11]. We investigate here the case of wires on top of a dielectric half space with permittivity ε_2 (assuming the center of the wires to be at $y = 0$ and the dielectric interface at $s = -h_2$) for the case of general ratios of wire radius to wire half spacing w to determine the transfer and self-elastances (elastance is the inverse of capacitance [18] and these elements are sometimes referred to as coefficients of potential [19, 20]). As mentioned immediately following Eq. (3), there is a practical case where only one dielectric interface is present, when the outer jacket material is absent ($\varepsilon_2 = \varepsilon_0$ different from ε_1). In the present section we have taken $\varepsilon_1 = \varepsilon_0$ different from ε_2 , but we could replace ε_2 by ε_1 to address this more practical situation.

The transfer elastance of the grid can be defined by [21]

$$S_{c,j} = \phi_{c,j}/(wq) = \phi_{c,j}/(2wD_0w), \quad (6)$$

where D_0 is the vertical displacement field below or above the wires; q is the charge; $\phi_{c,j}$ (the subscript j indicates internal, i , or external, e) is the difference of the electric potential at the point $y \rightarrow \pm\infty$ and a point on the wire, say at $x = 0, y = a$ or at $x = a, y = 0$. In a similar manner one could define the self elastance $S_{b,j}$ through the potential $\phi_{b,j}$, which is the counterpart of $\phi_{c,j}$ for the self-elastance computed as a limiting value in the illuminated half space with the uniform field contribution E_0 to the potential removed.

Assuming a drive from above, the potential can be written as

$$\begin{aligned} \phi \frac{2\pi\varepsilon_0}{q} &= c_0 - \sum_{m=0}^{\infty} \frac{p_m}{q} \operatorname{Re} \left[\frac{\partial^m}{\partial s^m} \left\{ \ln \left(e^{-i\pi(z+ih_2)/w} - e^{\pi s/w} \right) - \frac{\pi s}{2w} \right\} \right]_{s=h_2} \\ &- c_0 \frac{\varepsilon_0 - \varepsilon_2}{\varepsilon_0 + \varepsilon_2} - \frac{\varepsilon_0 - \varepsilon_2}{\varepsilon_0 + \varepsilon_2} \sum_{m=0}^{\infty} \frac{p_m}{q} \operatorname{Re} \left[\frac{\partial^m}{\partial s^m} \left\{ \ln \left(e^{-i\pi(z+ih_2)/w} - e^{-\pi s/w} \right) + \frac{\pi s}{2w} \right\} \right]_{s=h_2}, \quad y \geq -h_2 \\ \phi \frac{2\pi\varepsilon_2}{q} &= c_0 \frac{2\varepsilon_2}{\varepsilon_0 + \varepsilon_2} - \frac{2\varepsilon_2}{\varepsilon_0 + \varepsilon_2} \sum_{m=0}^{\infty} \frac{p_m}{q} \operatorname{Re} \left[\frac{\partial^m}{\partial s^m} \left\{ \ln \left(e^{-i\pi(z+ih_2)/w} - e^{\pi s/w} \right) - \frac{\pi s}{2w} \right\} \right]_{s=h_2}, \quad y \leq -h_2 \end{aligned} \quad (7)$$

where ε_0 is the absolute permittivity of free space, c_0 is a potential constant; p_m is the multipole moment (where the filament term is $m = 0$; the dipole term is $m = 1$; the quadrupole term is $m = 2$, etc.); p'_m is defined as $p_m \pi^m / (qw^m)$. We use as match points the points $z = -iae^{im'\pi/M}$, with $m' = 0, 1, \dots, M$, at which locations the potential is assumed to be a constant equal to zero to determine c_0 and p'_m with $m = 1, \dots, M$, and $p'_0 = 1$. A similar representation of the potential can be derived from a drive from below. The conformal mapping multipolar solution of the internal transfer elastance $S_{c,i}$ (see [21] for its derivation) is thus given by

$$(2\pi\varepsilon_0 w) S_{c,i} = -\frac{1}{\varepsilon_0 + \varepsilon_2} \left[(\varepsilon_2 - \varepsilon_0) \frac{\pi s}{w} + \varepsilon_2 p'_1 + 2\varepsilon_0 c_0 \right], \quad (8)$$

the one of the external self-elastance $S_{b,e}$ is given by

$$(2\pi\epsilon_0 w) S_{b,e} = \frac{\epsilon_0}{\epsilon_0 + \epsilon_2} \left[\left(1 - \frac{\epsilon_0}{\epsilon_2}\right) \frac{\pi s}{w} + p'_1 - 2c_0 \right], \quad (9)$$

the one of the external transfer elastance $S_{c,e}$ is given by

$$(2\pi\epsilon_0 w) S_{c,e} = -\frac{1}{\epsilon_0 + \epsilon_2} \left[(\epsilon_2 - \epsilon_0) \frac{\pi s}{w} - \epsilon_0 p'_1 + 2\epsilon_0 c_0 \right], \quad (10)$$

and the one of the internal self elastance $S_{b,i}$ is given by

$$(2\pi\epsilon_0 w) S_{b,i} = -\frac{1}{\epsilon_0 + \epsilon_2} \left[(\epsilon_2 - \epsilon_0) \frac{\pi s}{w} + \epsilon_2 p'_1 + 2\epsilon_0 c_0 \right], \quad (11)$$

where p'_1 is the dipole coefficient in the multipole representation of the potential and $s = h_2$.

4. NUMERICAL RESULTS FOR ONE-DIMENSIONAL ARRAY OF WIRES ON TOP OF A DIELECTRIC HALF SPACE

Consider the case of $\epsilon_1 = \epsilon_0$ and $\epsilon_2 = 2\epsilon_0$, with $h_1 = h_2 = a$. Using $\phi_{c,j}/E_0$ and $\phi_{b,j}/E_0$ and considering up to order $M = 0$ (filament), 1 (dipole), 2 (quadrupole), 3 (octupole) in the first principles method, we plot in Fig. 3 the internal and external transfer and self-elastances versus a/w as dark gray curves. One

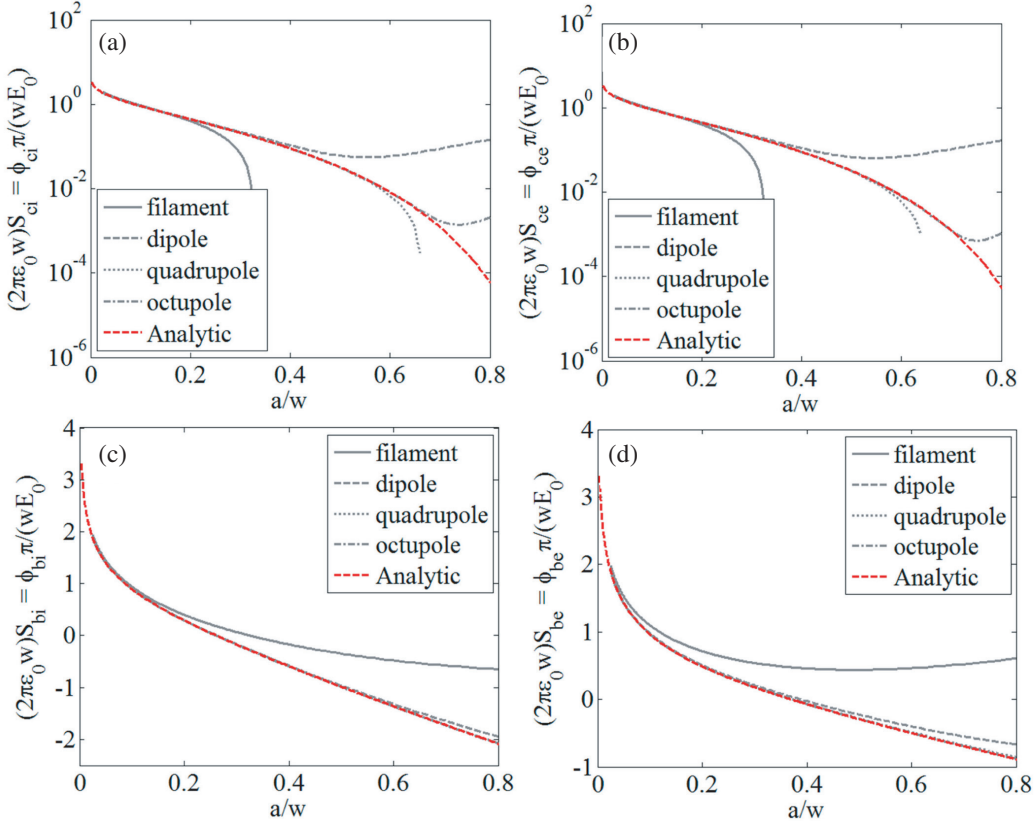


Figure 3. The elastance (a) $S_{c,i}$, (b) $S_{c,e}$, (c) $S_{b,i}$, and (d) $S_{b,e}$ of a wire grid versus the ratio a/w when $\epsilon_1 = \epsilon_0$, $\epsilon_2 = 2\epsilon_0$, and $h_1 = h_2 = a$. The red dashed line pertains to the analytical model that uses a multipole-conformal mapping expansion for the wire charges in Eqs. (8)–(11) including up to the $M = 8$ multipole. The dark gray lines pertain to the electric multipole first principles penetration model up to order $M = 0$ (filament), 1 (dipole), 2 (quadrupole), 3 (octupole).

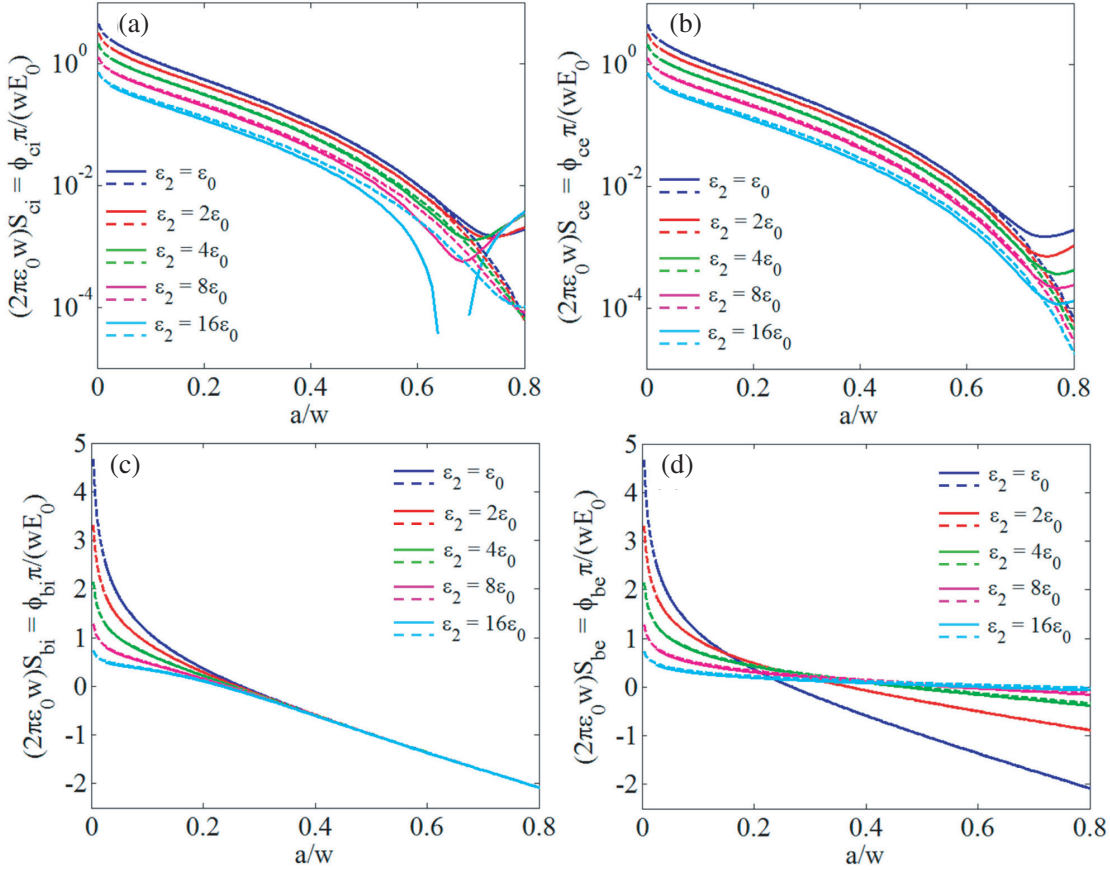


Figure 4. The elastance (a) $S_{c,i}$, (b) $S_{c,e}$, (c) $S_{b,i}$, and (d) $S_{b,e}$ of a wire grid versus the ratio a/w when $\varepsilon_1 = \varepsilon_0$, $\varepsilon_2 = \{\varepsilon_0, 2\varepsilon_0, 4\varepsilon_0, 8\varepsilon_0, 16\varepsilon_0\}$, and $h_1 = h_2 = a$. The dashed lines pertain to the analytical model that uses a multipole-conformal mapping expansion for the wire charges in Eqs. (8)–(11) including up to the $M = 8$ multipole. The solid lines pertain to the electric multipole first principles penetration model up to order $M = 3$ (octupole).

can notice that the agreement with the analytical conformal mapping solution reported as a red curve is best when using up to the octupole moment in the first principles method, covering a dynamic range of up to $a/w = 0.6$, within the characteristics of many commercial cables. As a/w decreases, the plots in Fig. 3 show that the transfer and self-elastances increase. In general, more accuracy can be obtained by increasing the number of multipoles, as it provides more means to model the charge distribution in each of the wire segments. However, the multipole moment formulas do become more complicated with increasing order.

Consider the same case as in Fig. 3, but now with various dielectric permittivities $\varepsilon_2 = \{\varepsilon_0, 2\varepsilon_0, 4\varepsilon_0, 8\varepsilon_0, 16\varepsilon_0\}$. Using $\phi_{c,j}/E_0$ and $\phi_{b,j}/E_0$ and considering up to order $M = 3$ (octupole) in the first principles method, we plot in Fig. 4 the internal and external transfer and self-elastances versus a/w as solid curves. These are compared to the conformal mapping solutions given as dashed lines. One can notice that the agreement with the analytical conformal mapping solution decreases with increasing dielectric constant, and, when using up to the octupole moment, covers a dynamic range of about to $a/w = 0.5 – 0.6$. We note however that common dielectric constants found in commercial cables range from $2\varepsilon_0$ to $4\varepsilon_0$, for which great agreement is observed.

Consider now $\varepsilon_1 = \varepsilon_0$ and $\varepsilon_2 = \{\varepsilon_0, 16\varepsilon_0\}$, with $h_1 = h_2 = \{a, 1.1a, 2a\}$. Using $\phi_{c,j}/E_0$ and $\phi_{b,j}/E_0$ and considering up to order $M = 3$ (octupole) in the first principles method, we plot in Fig. 5 the internal and external transfer and self-elastances versus a/w as solid curves. These are compared to the conformal mapping solutions given as dashed lines. One can notice that the potential constants

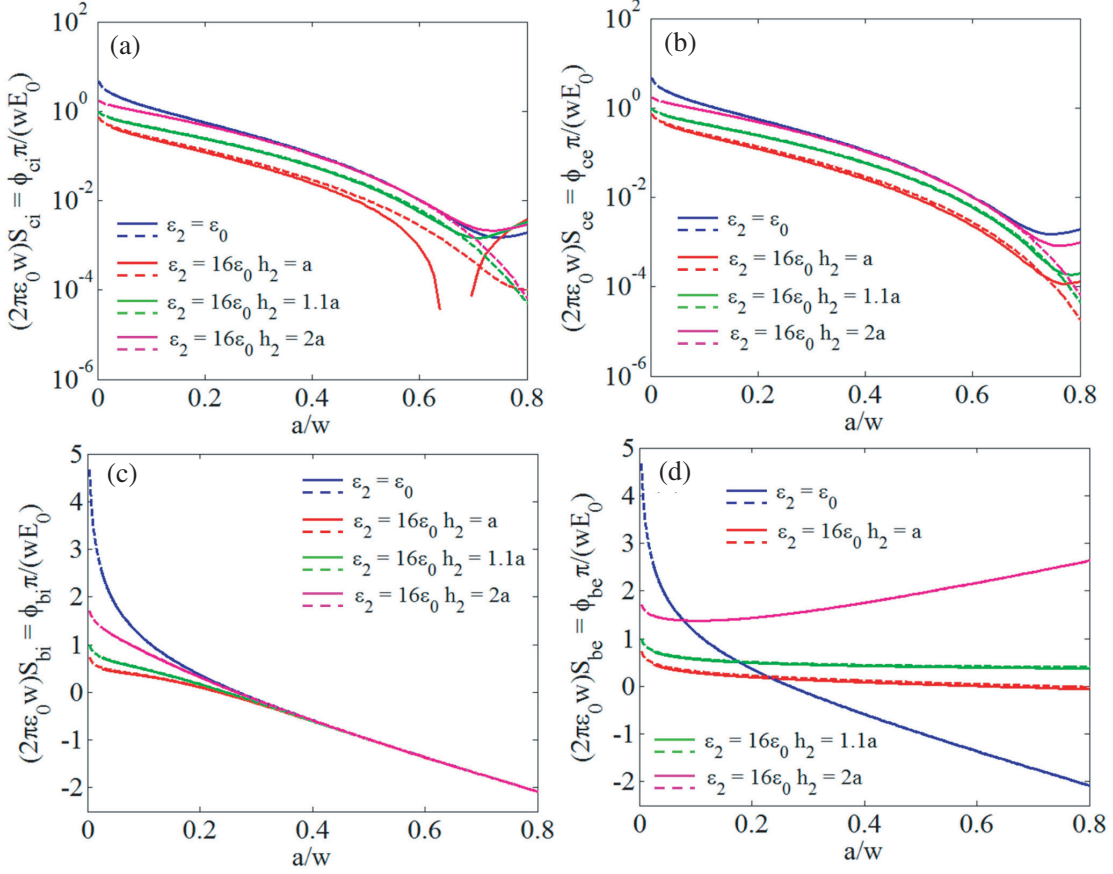


Figure 5. The elastance (a) $S_{c,i}$, (b) $S_{c,e}$, (c) $S_{b,i}$, and (d) $S_{b,e}$ of a wire grid versus the ratio a/w when $\epsilon_1 = \epsilon_0$, $\epsilon_2 = \{\epsilon_0, 16\epsilon_0\}$, and $h_1 = h_2 = \{a, 1.1a, 2a\}$. The dashed lines pertain to the analytical model that uses a multipole-conformal mapping expansion for the wire charges in Eqs. (8)–(11) including up to the $M = 8$ multipole. The solid lines pertain to the electric multipole first principles penetration model up to order $M = 3$ (octupole).

tend to be equal to the ones in free space when the interface is $2a$ away from the wires. We stress that the use of $\epsilon_2 = 16\epsilon_0$ is an exaggerated condition, and it is only used for clarity of explanation. We note that for the typical relative permittivities encountered (say, $2\epsilon_0 - 3\epsilon_0$), with typical a/w ratios (say, $1/5 - 1/1.3$), and with $2a$ the average meander distance from the dielectric interface, the elastance values for $S_{c,i}$, $S_{c,e}$, and $S_{b,i}$ are essentially the same as those of free space.

From Fig. 5(b), one can observe a dependence of $S_{b,e}$ on permittivity ϵ_2 . The total potential has an asymptotic form for $y \rightarrow -\infty$ as $\phi^{tot} \sim -(y-s)D_0/\epsilon_2 + \phi_{b,e}$. However, we recognize that the uniform electric field above the interface $y > -h_2$ is D_0/ϵ_0 rather than D_0/ϵ_2 . Hence, we could reconstruct a better approximation to the total potential as $\phi_0^{tot} \sim -(y-s)D_0/\epsilon_2 + \phi_{b,e}^0 + s(D_0/\epsilon_0 - D_0/\epsilon_2)$, $\phi_{b,e}^0$ is the potential computed for $\epsilon_2 = \epsilon_0$. Setting the two total potentials equal gives $\phi_{b,e} \sim \phi_{b,e}^0 + s(D_0/\epsilon_0 - D_0/\epsilon_2)$, and thus

$$(2\pi\epsilon_0 w) S_{b,e} \sim (2\pi\epsilon_0 w) S_{b,e}^0 + (1 - \epsilon_0/\epsilon_2) \pi (h_2/a) (a/w) \quad (12)$$

Here, we have taken $\epsilon_1 = \epsilon_0$ different from ϵ_2 , but we could also have ϵ_1 different from ϵ_0 , in which case an analogous correction to Eq. (12) would also apply to $S_{b,i}$.

Limiting our attention to $S_{b,e}$ for the case with $\epsilon_2 = 3\epsilon_0$, using $\phi_{b,e}/E_0$ and considering up to order $M = 3$ (octupole) in the first principles method, we plot in Fig. 6 the external self-elastance $S_{b,e}$ versus a/w as solid curves. These are compared to Eq. (12) given as dashed lines. One can notice that the corrected potential constants (dashed lines) tend to be equal to the multipole ones for sizeable a/w

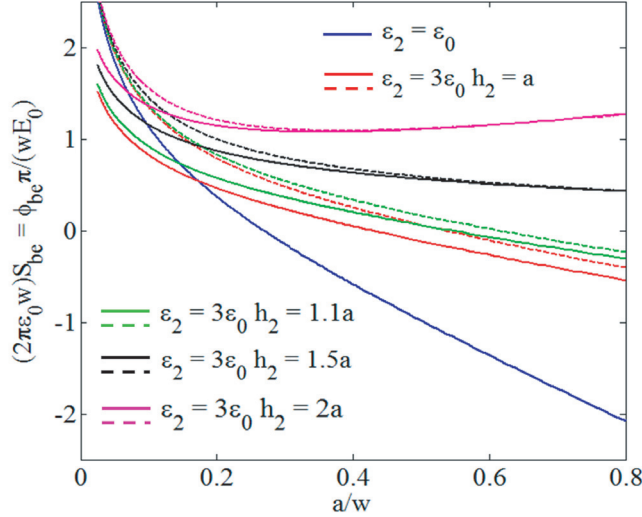


Figure 6. The elastance $S_{b,e}$ of a wire grid versus the ratio a/w when $\varepsilon_1 = \varepsilon_0$, $\varepsilon_2 = \{\varepsilon_0, 3\varepsilon_0\}$, and $h_1 = h_2 = \{a, 1.1a, 1.5a, 2a\}$. The dashed lines pertain to the correction in Eq. (12). The solid lines pertain to the electric multipole first principles penetration model up to order $M = 3$ (octupole).

when the interface is larger than $1.1a$ away from the wires. We note that Eq. (12) could be generalized to also work for small a/w by including more details of the imaged charges, but we prefer here to stick with the correction for the planar static mode alone.

5. FORMULAS TO EVALUATE TRANSFER AND SELF-CAPACITANCES IN THE PRESENCE OF DIELECTRICS

In the previous sections, we have described a method to calculate the potential constants $\phi_{c,i}$ and $\phi_{b,i}$. They will be used here to determine, for a uniform cylindrical braid above a ground plane, the transfer capacitance C_T and the self-capacitance C_1 . These capacitances are given by

$$C_1 = C_0 + \Delta C = \frac{2\pi\varepsilon_1}{\ln[(b + \phi_{b,i}/E_0)/a]} = \frac{2\pi\varepsilon_1}{\ln[(b + \varepsilon_1\phi_{b,i}/D_0)/a]} \quad (13)$$

$$C_T = \frac{\phi_{c,i}}{E_0} \frac{C_1 C_{sh}}{2\pi b \varepsilon_2} = \frac{\phi_{c,i}}{D_0} \frac{C_1 C_{sh}}{2\pi b},$$

where ΔC is a correction to the self-capacitance per unit length, $C_0 = 2\pi\varepsilon_1/\ln[b/a]$ assuming an infinitely extended dielectric (equations to compute the capacitance when the dielectric is a thin coating can be found in [22]), a and b are the inner and outer radii of a cylindrical coax (b usually taken as the mean braid radius), and, for a cylindrical shield h above a ground plane, $C_{sh} = 2\pi\varepsilon_2/\text{arccosh}[h/b]$. Note that the constant ϕ_c from the exterior uniform field in Fig. 5 of [6] is taken to impinge from above in the ε_2 region and thus corresponds to $\phi_{c,i}$ in Fig. 1(a) of this paper (Fig. 1 is rotated by one hundred eighty degrees from Fig. 5 of [6]).

6. CONCLUSION

In this paper, we reported the formulation to account for dielectrics in a first principles multipole-based cable braid electromagnetic penetration model. We used the formulation to model a one-dimensional array of wires, though the method is general and applicable to realistic cable geometries. The first principles results were compared to results retrieved analytically through a multipole-conformal mapping expansion for the wire charges. These results are found in good agreement up to a radius to half spacing ratio of 0.5–0.6, depending on the permittivity value of the dielectric used, within the characteristics

of many commercial cables. We further observed that for typical relative permittivities encountered in braided cables and with $2a$ the average meander distance from the dielectric interface, the transfer elastance values are essentially the same as those of free space; the self-elastance values are also derived from the free space solution as long as the dielectric discontinuity is taken into account for the planar mode. Our first principles model allows to account for the actual cable geometry, which is particularly useful if perturbations exist in the geometry versus nominal commercial braid parameters. In future work we will analyze the magnetic penetration case, which, in conjunction with the electric penetration case shown here, will provide a complete framework to model the response of realistic shielded cables.

ACKNOWLEDGMENT

Sandia National Laboratories is a multimission laboratory managed and operated by National Technology and Engineering Solutions of Sandia, LLC, a wholly owned subsidiary of Honeywell International, Inc., for the U.S. Department of Energy's National Nuclear Security Administration under contract DE-NA-0003525.

APPENDIX A. DECOMPOSITION OF THE PROBLEM AND DETERMINATION OF E_A IN THE CASE OF EXCITATION FROM BELOW

As was done in [11] in the absence of dielectrics, we decompose the problem of a field below the braid and zero electric field above the braid into the superposition of two problems as reported in Fig. A1.

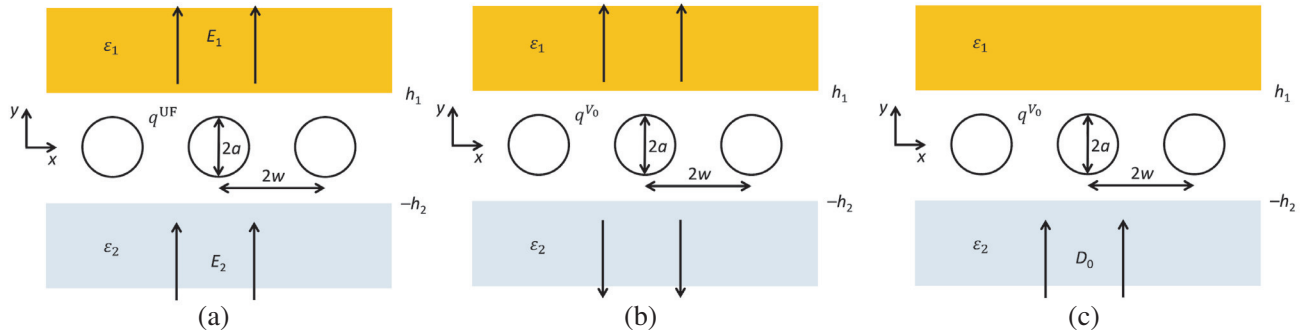


Figure A1. Decomposition of the problem into (a) a uniform-field problem for the total charge per unit-cell q^{UF} , and (b) a constant potential problem for the total charge per unit-cell q^{V_0} , to yield the solution with (c) a uniform incident field and an imposed potential on the braided shield based on the computed total charges from the uniform field problem and the constant potential problem.

The first problem is setup with a y -directed uniform incident field as in Eq. (1) and zero total potential on the braid surface as shown in Fig. A1(a). The uniform field is setup to have continuity of the normal electric displacement at each of the two interfaces. The total charge for a unit cell q^{UF} due to the uniform field excitation is computed (the superscript ‘UF’ refers to the uniform field solution for the braid problem). The second problem is setup with a constant potential V_0 on the braid as shown in Fig. A1(b). In that case the total charge for a unit cell q^{V_0} due to a constant potential is computed. The electric fields in the distant dielectric regions must obey Gauss’s law for the electric charges but are otherwise arbitrary and are taken to be equal and outward as $E_1 = \frac{q^{V_0}/A}{\epsilon_1 + \epsilon_2} = E_2$ (where A is the unit cell area). For the fields in the dielectric region above the braid to cancel to achieve the problem of Fig. A1(c), the fields in the two problems must be negative of one another, $E_1 = \frac{-q^{UF}/A}{\epsilon_1 + \epsilon_2} - \frac{\epsilon_0}{\epsilon_1} E_a$. Using the enforced relation $-D_0 = q^{V_0}/A + q^{UF}/A$, we obtain $E_1 = \frac{q^{V_0}/A}{\epsilon_1 + \epsilon_2} = \frac{D_0 + q^{V_0}/A}{\epsilon_1 + \epsilon_2} - \frac{\epsilon_0}{\epsilon_1} E_a$, for which $\frac{D_0}{\epsilon_1 + \epsilon_2} = \frac{\epsilon_0}{\epsilon_1} E_a$, leading to $\epsilon_0 E_a = \frac{\epsilon_1 D_0}{\epsilon_1 + \epsilon_2}$.

REFERENCES

1. Vance, E. F., *Coupling to Shielded Cables*, R. E. Krieger, 1987.
2. Celozzi, S., R. Araneo, and G. Lovat, *Electromagnetic Shielding*, John Wiley and Sons, 2008.
3. Lee, K. S. H., *EMP Interaction: Principles, Techniques, and Reference Data*, Hemisphere Publishing Corp., Washington, 1986.
4. Tesche, F. M., M. V. Ianoz, and T. Karlsson, *EMC Analysis Methods and Computational Models*, John Wiley & Sons, Inc., New York, 1997.
5. Warne, L. K., W. L. Langston, L. I. Basilio, and W. A. Johnson, "Cable braid electromagnetic penetration model," *Sandia National Laboratories Report*, SAND2015-5019, Albuquerque, NM, 2015.
6. Warne, L. K., W. L. Langston, L. I. Basilio, and W. A. Johnson, "First principles cable braid electromagnetic penetration model," *Progress In Electromagnetics Research B*, Vol. 66, 63–89, 2016.
7. Campione, S., L. I. Basilio, L. K. Warne, H. G. Hudson, and W. L. Langston, "Shielding effectiveness of multiple-shield cables with arbitrary terminations via transmission line analysis," *Progress In Electromagnetics Research C*, Vol. 65, 93–102, 2016.
8. Demoulin, B., P. Degauque, M. Cauterman, and R. Gabillard, "Shielding performance of triply shielded coaxial cables," *IEEE Transactions on Electromagnetic Compatibility*, Vol. 22, 173–180, 1980.
9. Lee, K. S. H. and C. F. Baum, "Application of modal analysis to braided-shield cables," *IEEE Transactions on Electromagnetic Compatibility*, Vol. 17, 159–169, 1975.
10. Johnson, W. A., L. K. Warne, L. I. Basilio, R. S. Coats, J. D. Kotulski, and R. E. Jorgenson, "Modeling of braided shields," *Proceedings of Joint 9th International Conference on Electromagnetics in Advanced Applications ICEAA 2005 and 11th European Electromagnetic Structures Conference EESE*, 881–884, Torino, Italy, 2005.
11. Campione, S., L. K. Warne, W. L. Langston, W. A. Johnson, R. S. Coats, and L. I. Basilio, "Multipole-based cable braid electromagnetic penetration model: Electric penetration case," *IEEE Transactions on Electromagnetic Compatibility*, Vol. 60, 444–452, 2018.
12. Kley, T., "Optimized single-braided cable shields," *IEEE Transactions on Electromagnetic Compatibility*, Vol. 35, 1–9, 1993.
13. Takashima, T. and R. Ishibashi, "Electric fields in dielectric multi-layers calculated by digital computer," *IEEE Transactions on Electrical Insulation*, Vol. 13, 37–44, 1978.
14. Landau, L. D. and E. M. Lifshitz, *Electrodynamics of Continuous Media*, 2nd Edition, Pergamon Press, 1984.
15. Langmuir, R. V., *Electromagnetic Fields and Waves*, McGraw Hill, 1961.
16. Larsen, T., "A Survey of the theory of wire grids," *IRE Transactions on Microwave Theory and Techniques*, Vol. 10, 191–201, 1962.
17. Casey, K. F., "Electromagnetic shielding behavior of wire-mesh screens," *IEEE Transactions on Electromagnetic Compatibility*, Vol. 30, 298–306, 1988.
18. Smythe, W. R., *Static and Dynamic Electricity*, Hemisphere Publishing Corp., New York, 1989.
19. Schelkunoff, S. A., *Electromagnetic Waves*, D. Van Nostrand Company, Inc., New York, NY, 1943.
20. Ramo, S., J. R. Whinnery, and R. V. Duzer, *Fields and Waves in Communication Electronics*, John Wiley & Sons, Inc., New York, NY, 1965.
21. Warne, L. K., W. L. Langston, and S. Campione, "Approximations to wire grid elastance," *Sandia National Laboratories Report*, SAND2016-6180, Albuquerque, NM, 2016.
22. Campione, S., L. K. Warne, L. I. Basilio, C. D. Turner, K. L. Cartwright, and K. C. Chen, "Electromagnetic pulse excitation of finite- and infinitely-long lossy conductors over a lossy ground plane," *Journal of Electromagnetic Waves and Applications*, Vol. 31, 209–224, 2017.